# Electromagnetic Plane Wave Excitation of an Open-Ended Conducting Frustum

Anthony M. J. Davis and Robert W. Scharstein, *Senior Member, IEEE*

***Abstract*—A Chebyshev-Galerkin solution of the electric field integral equation for the surface current induced on a conducting frustum by an incident plane wave is presented. The physically motivated mathematics takes proper account of the static singularity in the kernel function and of the edge conditions at both apertures, to yield complete and convergent current expansions. Coupling of the electromagnetic field into the tapered interior of the open scatterer can be substantial, even in electrically narrow cross sections, due to the focusing action of the conical transmission line.**

## I. Introduction

A MIXED boundary value problem is formulated for the surface currents that are induced by a time-harmonic plane wave incident upon an open-ended conductor whose shape is a frustum, namely a finite-length portion of a cone (Fig. 1). Scattered fields are represented in terms of the uncoupled azimuthal Fourier modes of this body of revolution. Physically, the scattering may be regarded as a distortion of that previously determined [1] for an open-ended tube since the same essential features must be exhibited. This reasoning provides an appropriate mathematical formulation for this more complicated geometry. Thus, after a suitable change of the radial coordinate, the integral equation for the surface currents can be reduced, for each azimuthal mode, to a set of linear equations by means of a Galerkin expansion of the currents in terms of Chebyshev polynomials with edge-condition weighting.

Because this Galerkin procedure uses a complete set of orthogonal basis functions, the kernel of the integral equation (which involves the free-space Green's function) is directly expanded in the efficient spirit of Lee [2], [3] into a dual series of Chebyshev polynomials. The coefficients in the set of linear equations are efficiently computed as triple Fourier coefficients, upon the extraction and careful treatment of the important static singularity. Inclusion of the proper edge conditions ensures the rapid convergence of the Chebyshev series for the currents. Resultant surface currents and axial electric fields are graphed and interpreted for two different frustra, when energized from several angles of incidence.

Manuscript received September 2, 1993; revised December 3, 1993. This work was supported by the Weapons Sciences Directorate, US Army Missile Command, Redstone Arsenal, AL, under Contract DAAH01-91-D-R001, Delivery Order 7.

A. M. J. Davis is with the Mathematics Department, University of Alabama, Tuscaloosa, AL 35487-0350 USA.

R. W. Scharstein is with the Electrical Engineering Department, University of Alabama, Tuscaloosa, AL 35487-0286 USA.

IEEE Log Number 9401345.

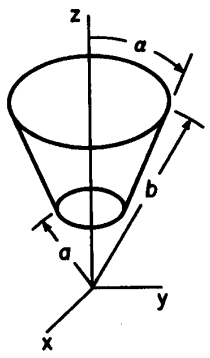


Fig. 1. Frustum geometry.

This open frustum is simple enough to be an important canonical scatterer because of the variable surface curvature and the aperture and edge effects. The exterior problem for scattering by an infinite cone is the subject of much research (for example, see [4]). Determination of the propagation characteristics of the conical transmission line is a standard eigenvalue problem [5], [6]. As in the case of the circular tube [1], the standing wave nature of the surface currents indicates that the interaction between the exciting plane wave and the frustum ends occurs via the external surface and internal guided waves of the nonuniform waveguide.

## II. The Scattering of a TM Wave

A sinusoidal electromagnetic wave of period $2\pi/\omega$ is incident on a hollow, infinitesimally thin, and perfectly conducting frustum cut from a cone of angle $\alpha$ (Fig. 1). Choose spherical polar coordinates $(r, \theta, \phi)$ so that the conducting frustum is at $\theta = \alpha, a \le r \le b$. Also, with $(x, y) = r \sin\theta(\cos\phi, \sin\phi)$, $z = r\cos\theta$, define $\hat{\mathbf{r}}, \hat{\theta}, \hat{\phi}, \hat{\mathbf{x}}, \hat{\mathbf{y}}$ and $\hat{\mathbf{z}}$ to be unit vectors associated with these polar and Cartesian coordinates.

With the time factor $e^{-i\omega t}$ suppressed, Maxwell's equations in free space allow the representation

$$\mathbf{H} = \nabla \times \mathbf{A}, \qquad \mathbf{E} = ik\eta\mathbf{A} - \nabla\Phi \tag{1}$$

in terms of vector and scalar potentials $\mathbf{A}$ and $\Phi$ that satisfy the Helmholtz equation and are related by

$$\nabla \cdot \mathbf{A} = i\frac{k}{\eta}\Phi. \tag{2}$$

The incident and scattered wave fields are thus determined, respectively, by $\mathbf{A}^i$ and $\mathbf{A}^s$. Suppose that a TM wave, polar-

ized with the magnetic field parallel to $\hat{\mathbf{y}}$, is incident from the direction that makes an angle $\beta$ with $\hat{\mathbf{z}}$. Then,

$$\mathbf{E}^i = E^{0i}(\hat{\mathbf{z}}\sin\beta - \hat{\mathbf{x}}\cos\beta) \cdot\exp[-ik(x\sin\beta + z\cos\beta)] = ik\eta\mathbf{A}^i. \quad (3)$$

Now the scattered field may be regarded as due to surface currents $\mathbf{J}_S$ on the frustum. When these are identified, according to (1), with the discontinuities in the normal derivatives of $\mathbf{A}^s$, it follows that

$$\mathbf{A}^s(\mathbf{r}) = \int\int_S \mathbf{J}_S(\mathbf{r}')G(\mathbf{r},\mathbf{r}')dS', \quad (4)$$

where $S$ denotes the frustum and the free-space Green's function is given by

$$G(\mathbf{r},\mathbf{r}') = \frac{e^{ik|\mathbf{r}-\mathbf{r}'|}}{4\pi|\mathbf{r}-\mathbf{r}'|}. \quad (5)$$

The substitution of (4) into (2) and (1) then yields, after some standard manipulations, an expression for the scattered electric field $\mathbf{E}^s$, from which the electric field integral equation [7]

$$\hat{\mathbf{n}}\times\mathbf{E}^i(\mathbf{r}) = \frac{\eta}{ik}\hat{\mathbf{n}}\times\int\int_S [k^2\mathbf{J}_S(\mathbf{r}')G(\mathbf{r},\mathbf{r}') - \nabla'\cdot\mathbf{J}_S(\mathbf{r}')\nabla'G(\mathbf{r},\mathbf{r}')]dS' \quad (\mathbf{r}\in S) \quad (6)$$

may be derived by requiring the tangential components of the total electric field to vanish. For the frustum, $\hat{\mathbf{n}} = \hat{\theta}$ and $dS' = r'\sin\alpha\, dr'd\phi'$. Thus, on writing

$$\mathbf{J}_S(\mathbf{r}) = J_{Sr}\hat{\mathbf{r}} + J_{S\phi}\hat{\phi}, \quad (7)$$

the three terms in (6) may be written as

$$\hat{\mathbf{n}}\times\mathbf{E}^i = E^{0i}[\hat{\phi}(\cos\beta\sin\alpha\cos\phi - \sin\beta\cos\alpha) + \hat{\mathbf{r}}\cos\beta\sin\phi]\cdot\exp[-ikr(\sin\beta\sin\alpha\cos\phi + \cos\beta\cos\alpha)], \quad (8)$$

$$-ik\eta\hat{\mathbf{n}}\times\int\int_S \mathbf{J}_S(\mathbf{r}')G(\mathbf{r},\mathbf{r}')dS' = ik\eta\sin\alpha\int_{-\pi}^{\pi}\int_a^b G(\mathbf{r},\mathbf{r}')\cdot\Big[\hat{\phi}J_{Sr}(\sin^2\alpha\cos(\phi-\phi') + \cos^2\alpha) + J_{S\phi}\sin\alpha\sin(\phi-\phi')] + \hat{\mathbf{r}}[J_{Sr}\sin\alpha\sin(\phi-\phi') - J_{S\phi}\cos(\phi-\phi')]\Big]r'dr'd\phi', \quad (9)$$

$$-\frac{\eta}{ik}\hat{\mathbf{n}}\times\int\int_S \nabla'\cdot\mathbf{J}_S(\mathbf{r}')\nabla'G(\mathbf{r},\mathbf{r}')dS' = -\frac{\eta}{ik}\int_{-\pi}^{\pi}\int_a^b\left[\frac{\sin\alpha}{r'}\frac{\partial}{\partial r'}(r'^2J_{Sr}) + \frac{\partial J_{S\phi}}{\partial\phi'}\right]\cdot\left[\hat{\phi}\frac{\partial G}{\partial r} - \frac{\hat{\mathbf{r}}}{r\sin\alpha}\frac{\partial G}{\partial\phi}\right]dr'd\phi'. \quad (10)$$

Now, when $\mathbf{r}$ and $\mathbf{r}'$ lie on the frustum, as in (6), their separation distance $R$ is given by

$$R = |\mathbf{r}-\mathbf{r}'| = \left[(r-r')^2 + 4rr'\sin^2\alpha\sin^2\left(\frac{\phi-\phi'}{2}\right)\right]^{1/2}. \quad (11)$$

Hence the Green's function (5) has a Fourier series expansion of the form

$$G = G_0 + 2\sum_{n=1}^{\infty}G_n\cos n(\phi-\phi') \quad (12)$$

in which the coefficients depend on $k$ and the distances $|r-r'|$ and $(rr')^{1/2}\sin\alpha$. Comparison of (8) and (10) then shows that the surface currents in (7) must have the azimuthal structure

$$J_{Sr} = \frac{4E^{0i}}{\pi\eta}\left[j_{r0}(r') + 2\sum_{m=1}^{\infty}(-i)^m j_{rm}(r')\cos m\phi'\right]$$
$$J_{S\phi} = \frac{8E^{0i}}{\pi\eta}\sum_{m=1}^{\infty}(-i)^m j_{\phi m}(r')\sin m\phi' \quad (13)$$

in which the radially varying coefficients are dimensionless. Thus, after noting that (8) involves $\beta$ and $\phi$ derivatives of the expansion

$$\exp(-ikr\sin\beta\sin\alpha\cos\phi) = J_0(kr\sin\beta\sin\alpha) + 2\sum_{n=1}^{\infty}(-i)^n J_n(kr\sin\beta\sin\alpha)\cos n\phi \quad (14)$$

and substituting (12) and (13) into (9) and (10), the integral equation (6) on the frustum can be reduced, by suitable manipulation, to an infinite set of integral equations for the modal components of the surface currents, namely

$$\begin{aligned}
&-k^2\sin\alpha\int_a^b j_{r0}[G_0\cos^2\alpha + G_1\sin^2\alpha]r'dr' \\
&+\sin\alpha\int_a^b j_{r0}(r'\frac{\partial}{\partial r'} - 1)\frac{\partial G_0}{\partial r}dr' \\
&= \frac{k}{8}e^{-ikr\cos\beta\cos\alpha}[\cos\beta\sin\alpha J_1(kr\sin\beta\sin\alpha) \\
&\quad - i\sin\beta\cos\alpha J_0(kr\sin\beta\sin\alpha)], \\
&-k^2\sin\alpha\int_a^b [j_{rn}[2G_n\cos^2\alpha + (G_{n+1}+G_{n-1})\sin^2\alpha] \\
&+ j_{\phi n}(G_{n+1}-G_{n-1})\sin\alpha]r'dr' \\
&+2\frac{\partial}{\partial r}\int_a^b\left[j_{rn}(r'\frac{\partial}{\partial r'} - 1)G_n\sin\alpha - j_{\phi n}nG_n\right]dr' \\
&= \frac{k}{8}e^{-ikr\cos\beta\cos\alpha}[\cos\beta\sin\alpha[J_{n+1}(kr\sin\beta\sin\alpha) \\
&\quad - J_{n-1}(kr\sin\beta\sin\alpha)] \\
&\quad - 2i\sin\beta\cos\alpha J_n(kr\sin\beta\sin\alpha)] \qquad (n\geq 1), \\
&-k^2\sin\alpha\int_a^b [j_{rn}(G_{n+1}-G_{n-1})\sin\alpha \\
&\quad + j_{\phi n}(G_{n+1}+G_{n-1})]r'dr' \\
&-\frac{2n}{r\sin\alpha}\int_a^b\left[j_{rn}(r'\frac{\partial}{\partial r'} - 1)G_n\sin\alpha - j_{\phi n}nG_n\right]dr' \\
&= \frac{k}{8}e^{-ikr\cos\beta\cos\alpha}\cos\beta[J_{n+1}(kr\sin\beta\sin\alpha) \\
&\quad + J_{n-1}(kr\sin\beta\sin\alpha)] \quad (n\geq 1).
\end{aligned} \quad (15)$$

These equations, respectively, arise from the $\hat{\phi}, \hat{\phi}\cos n\phi$ and $\hat{\mathbf{r}}\sin n\phi$ terms in (6). They can be simplified by defining a new

variable that is a multiple of $\ln r$ and scaled, for convenience, so that its range is $-1$ to 1. Thus, multiply equations (15) by $r\sin\alpha$ and write

$$r^2 = (ab)\left[\frac{b}{a}\right]^s, \qquad \text{i.e.,} \qquad r\frac{\partial}{\partial r} = \frac{2}{\ln(b/a)}\frac{\partial}{\partial s}, \tag{16}$$

with $s'$ similarly related to $r'$. Then the unknown coefficients appear in the form $r'j_{r0}(r')\sin\alpha$, etc., and the kernel functions frequently contain the Fourier coefficients of $\mathcal{G} = k^2rr'G\sin^2\alpha$. The $\sin\alpha$ factors are superfluous at this stage but are included for proper recovery of earlier results for the finite circular cylinder [1] in the limit $\sin\alpha \to 0, a\sin\alpha \to A, b-a \to 2L$. Then $\ln(b/a) \sim \frac{2L}{A}\sin\alpha$ and (16) implies that $\frac{\partial}{\partial r} \sim L^{-1}\frac{\partial}{\partial s}$ so that $s$ coincides with $z/L$ in this limit. This observation also suggests that an aspect ratio $d$ of the frustum be introduced by defining

$$d = \frac{2\sin\alpha}{\ln(b/a)}. \tag{17}$$

The scattered field due to the frustum may be regarded as merely a distortion of that generated by the finite circular cylinder. In particular, the edge behavior of the surface currents is of the same type and hence the previously used expansions [1] remain valid. Thus, with $s' = \cos v'$, write

$$r'j_{rn}(r') = (ab)^{1/2}d\sum_{p=0}^{\infty} j_{rn}^p \sin(p+1)v' \qquad (n \geq 0)$$

$$r'j_{\phi n}(r') = \frac{(ab)^{1/2}d}{\sin v'}\sum_{p=0}^{\infty} j_{\phi n}^p \cos pv' \qquad (n \geq 1). \tag{18}$$

Also, introduce symmetric expansions of the Green's function components in terms of Chebyshev polynomials, defined by $T_p(\cos v) = \cos pv$, by writing

$$G_n = \frac{1}{(ab)^{1/2}\sin\alpha}\sum_{p,q=0}^{\infty}\epsilon_p\epsilon_q G_n^{p,q}T_p(s)T_q(s')$$

$$\mathcal{G}_n = k^2rr'G_n\sin^2\alpha = \frac{1}{(ab)^{1/2}\sin\alpha} \cdot \sum_{p,q=0}^{\infty}\epsilon_p\epsilon_q\mathcal{G}_n^{p,q}T_p(s)T_q(s') \quad (n \geq 0) \tag{19}$$

where $\epsilon_p$ is Neumann's symbol, equal to 1 if $p = 0$ and 2 otherwise. The length factors in (18) and (19) ensure that the new cofficients are dimensionless. Equations (15) can now be transformed by using (16) to replace $r, r'$ by $s, s'$ and substituting the expansions (18) and (19). The $s'$ integrals are readily evaluated and then consideration of the $U_p(s) = \sin(p+1)v/\sin v$ terms in the $\hat{\phi}, \hat{\phi}\cos n\phi$ equations of (15) and the $T_p(s)$ terms in the $\hat{\mathbf{r}}\sin n\phi$ equations yields, after some lengthy algebra, the following infinite linear system of equations for the unknown coefficients in each modal expansion in (18):

$$\sum_{q=0}^{\infty} j_{r0}^q\Big[2d^2(p+1)(q+1)G_0^{p+1,q+1} - d(p+1)\sin\alpha(G_0^{p+1,q} - G_0^{p+1,q+2}) - \frac{1}{2}(\mathcal{G}_0^{p,q} - \mathcal{G}_0^{p+2,q} - \mathcal{G}_0^{p,q+2} + \mathcal{G}_0^{p+2,q+2})\cos^2\alpha - \frac{1}{2}(\mathcal{G}_1^{p,q} - \mathcal{G}_1^{p+2,q} - \mathcal{G}_1^{p,q+2} + \mathcal{G}_1^{p+2,q+2})\sin^2\alpha\Big]$$
$$= \frac{1}{4\pi^2}\int_0^{\pi} dv\,\sin(p+1)v\sin v\,kr\sin\alpha\,e^{-ikr\cos\beta\cos\alpha} \cdot [\cos\beta\sin\alpha J_1(kr\sin\beta\sin\alpha) - i\sin\beta\cos\alpha J_0(kr\sin\beta\sin\alpha)] \quad (p \geq 0), \tag{20}$$

$$\sum_{q=0}^{\infty} j_{rn}^q\Big[2d^2(p+1)(q+1)G_n^{p+1,q+1} - d(p+1)\sin\alpha(G_n^{p+1,q} - G_n^{p+1,q+2}) - \frac{1}{2}(\mathcal{G}_n^{p,q} - \mathcal{G}_n^{p+2,q} - \mathcal{G}_n^{p,q+2} + \mathcal{G}_n^{p+2,q+2})\cos^2\alpha - \frac{1}{4}(\mathcal{G}_{n-1}^{p,q} - \mathcal{G}_{n-1}^{p+2,q} - \mathcal{G}_{n-1}^{p,q+2} + \mathcal{G}_{n-1}^{p+2,q+2} + \mathcal{G}_{n+1}^{p,q} - \mathcal{G}_{n+1}^{p+2,q} - \mathcal{G}_{n+1}^{p,q+2} + \mathcal{G}_{n+1}^{p+2,q+2})\sin^2\alpha\Big] - \sum_{q=0}^{\infty} j_{\phi n}^q\Big[2dn(p+1)G_n^{p+1,q} - \frac{1}{2}(\mathcal{G}_{n-1}^{p,q} - \mathcal{G}_{n-1}^{p+2,q} - \mathcal{G}_{n+1}^{p,q} + \mathcal{G}_{n+1}^{p+2,q})\sin\alpha\Big]$$
$$= \frac{1}{4\pi^2}\int_0^{\pi} dv\sin(p+1)v\sin v\,kr\sin\alpha\,e^{-ikr\cos\beta\cos\alpha} \cdot \Big[\frac{1}{2}\cos\beta\sin\alpha[J_{n+1}(kr\sin\beta\sin\alpha) - J_{n-1}(kr\sin\beta\sin\alpha)] - i\sin\beta\cos\alpha J_n(kr\sin\beta\sin\alpha)\Big] \quad (p \geq 0) \text{ for each } n \geq 1, \tag{21}$$

$$-\sum_{q=0}^{\infty} j_{rn}^q\Big[2dn(q+1)G_n^{p,q+1} - n\sin\alpha(G_n^{p,q} - G_n^{p,q+2}) - \frac{1}{2}(\mathcal{G}_{n-1}^{p,q} - \mathcal{G}_{n+1}^{p,q} - \mathcal{G}_{n-1}^{p,q+2} + \mathcal{G}_{n+1}^{p,q+2})\sin\alpha\Big] + \sum_{q=0}^{\infty} j_{\phi n}^q\Big[2n^2G_n^{p,q} - (\mathcal{G}_{n-1}^{p,q} + \mathcal{G}_{n+1}^{p,q})\Big]$$
$$= \frac{\cos\beta}{8\pi^2}\int_0^{\pi} dv\cos pv\,kr\sin\alpha\,e^{-ikr\cos\beta\cos\alpha} \cdot [J_{n+1}(kr\sin\beta\sin\alpha) + J_{n-1}(kr\sin\beta\sin\alpha)] \quad (p \geq 0) \text{ for each } n \geq 1. \tag{22}$$

Equations (20) determine $j_{r0}^q (q \geq 0)$, i.e., the axisymmetric component of $J_{Sr}$, according to (13) and (18). Meanwhile (21) and (22) form, for each azimuthal mode determined by $n$, a coupled linear system for $j_{rn}^q, j_{\phi n}^q (q \geq 0)$. These correspond to the systems given by the authors [1] for the finite circular cylinder and agreement can be demonstrated in the appropriate limit, described above.

The computation of the coefficients in (20)–(22) requires, according to (12) and (19), triple Fourier series expansions but care is again needed for the singularity in (5). Thus, consider

$$(G_n)_{k=0} = \frac{1}{4\pi^2}\int_0^{\pi}\frac{\cos n(\phi-\phi')}{R}d\phi$$

$$= \frac{1}{(ab)^{1/2}\sin\alpha}\sum_{p,q=0}^{\infty}\epsilon_p\epsilon_q F_n^{p,q}T_p(s)T_q(s')$$

$$k^2rr'(G_n)_{k=0}\sin^2\alpha = \frac{1}{(ab)^{1/2}\sin\alpha}\sum_{p,q=0}^{\infty}\epsilon_p\epsilon_q\mathcal{F}_n^{p,q}T_p(s)T_q(s')(n\geq 0), \tag{23}$$

where the distance $R$ is defined by (11). Now $(G_n)_{k=0}$ can be expressed in terms of an associated Legendre (toroidal) function [8], and hence

$$\left[\frac{ab}{rr'}\right]^{1/2}Q_{n-1/2}\left[1+\frac{(r-r')^2}{2rr'\sin^2\alpha}\right] = 4\pi^2\sum_{p,q=0}^{\infty}\epsilon_p\epsilon_q F_n^{p,q}T_p(s)T_q(s'). \tag{24}$$

Then, on defining $w = \frac{1}{4}\ln(b/a)$, it follows from (16) that

$$\frac{rr'}{ab} = e^{2w(s+s')}$$

and so the exact contribution of the singular term in $Q_{n-1/2}$ to each expansion is determined by noting that

$$\left[\frac{ab}{rr'}\right]^{1/2}\ln\left[\frac{1}{2|s-s'|}\right] = \sum_{p,q=0}^{\infty}\epsilon_p\epsilon_q(-1)^{p+q}L^{p,q}T_p(s)T_q(s')$$

where

$$L^{p,q} = \sum_{m=1}^{\infty}\frac{1}{2m}[I_{m+p}(w)+I_{|m-p|}(w)][I_{m+q}(w)+I_{|m-q|}(w)].$$

The corresponding contributions to $F_n^{p,q}$ and $\mathcal{F}_n^{p,q}$ in (23) are readily seen to be

$$\frac{(-1)^{p+q}}{4\pi^2}L^{p,q} \quad \text{and} \quad \frac{k^2ab\sin^2\alpha}{4\pi^2}L^{p,q}$$

respectively. After inserting the factor $e^{-w(s+s')}$, as in (24), or its counterpart $e^{w(s+s')}k^2ab\sin^2\alpha$, the remaining contributions can be computed from the regular functions

$$\ln\left[\frac{r-r'}{(s-s')(ab)^{1/2}\sin\alpha}\right] = \ln\left[\frac{e^{2ws}-e^{2ws'}}{2wd(s-s')}\right]$$

and

$$Q_{n-1/2}(\cosh 2\xi)+\ln\frac{2|r-r'|}{(ab)^{1/2}\sin\alpha} = \frac{\Gamma(n+\frac{1}{2})\Gamma(\frac{1}{2})}{\Gamma(n+1)}\cdot e^{-(2n+1)\xi}F\left(\frac{1}{2},n+\frac{1}{2};n+1,e^{-4\xi}\right)+\ln\frac{2|r-r'|}{(ab)^{1/2}\sin\alpha}$$

where $d$ is defined by (17) and

$$\sinh\xi = \frac{|r-r'|}{2(rr')^{1/2}\sin\alpha}.$$

Now, for any $n\geq 0$, the standard expansion of the above hypergeometric function $F$ in powers of $e^{-4\xi}$ converges geometrically for any $\xi>0$ but diverges logarithmically as $\xi\to 0$. Hence, for suitably small values of $\xi$, the following expansion, deduced from equation 15.3.10 of [9], is appropriate:

$$\begin{aligned}Q_{n-1/2}(\cosh 2\xi)+\ln\frac{2|r-r'|}{(ab)^{1/2}\sin\alpha} &= [1-e^{-(2n+1)\xi}]\ln\frac{2|r-r'|}{(ab)^{1/2}\sin\alpha}\\ &+ e^{-(2n+1)\xi}\left[\ln\left(\frac{16}{\cosh\xi}\right)+2\xi+w(s+s')-C_{0n}\right]\\ &+ e^{-(2n+1)\xi}\sum_{p=1}^{\infty}\frac{\Gamma(p+\frac{1}{2})\Gamma(p+n+\frac{1}{2})}{\Gamma(\frac{1}{2})\Gamma(n+\frac{1}{2})}\\ &\cdot\frac{(1-e^{-4\xi})^p}{(p!)^2}\left[\ln\left(\frac{16}{1-e^{-4\xi}}\right)-C_{pn}\right]\end{aligned}$$

where

$$C_{pn} = 2\sum_{m=p+1}^{p+n}\frac{1}{2m-1}+2\sum_{m=1}^{p}\frac{1}{m(2m-1)}.$$

The computations were checked by using the following alternative representation, valid for all $\xi>0$:

$$\begin{aligned}Q_{n-1/2}(\cosh 2\xi)+\ln\frac{2|r-r'|}{(ab)^{1/2}\sin\alpha} &= 3\ln 2-2\sum_{m=1}^{n}\frac{1}{2m-1}+\ln\left[\frac{(r-r')^2+4rr'\sin^2\alpha}{ab\sin^2\alpha}\right]^{1/2}\\ &-\int_0^1\frac{(1-u\tanh\xi)^{n-1/2}-1}{u}du\\ &+\ln\coth\xi\int_0^1\left[(\cosh 2\xi-\cosh^2\xi[(\tanh\xi)^{1-u}\right.\\ &\left.+(\tanh\xi)^{1+u}])^{n-1/2}-[1-(\tanh\xi)^{1-u}]^{n-1/2}\right]du.\end{aligned}$$

## III. The Scattered Field on the Frustum Axis

With the surface currents determined by (13) and (18) after solving (20)–(22), the scattered electric and magnetic fields are then obtained by substitution of (4) into (2) and then (1). For points $\mathbf{r}$ on the semiaxis $\theta=0$, which passes through the interior of the frustum, let the separation distance in (5) be defined by

$$R_0 = |\mathbf{r}-\mathbf{r}'| = (r^2+r'^2-2rr'\cos\theta')^{1/2}. \tag{25}$$

Then, since $G$ depends only on $(\mathbf{r}-\mathbf{r}')$, the vector derivatives can be readily transferred from $\mathbf{r}$ to $\mathbf{r}'$ to yield

$$\mathbf{H}^s(r,0) = \int\int_S \mathbf{J}_S(\mathbf{r}')\times\nabla' G(R_0)dS', \tag{26}$$

$$\mathbf{E}^s(r,0) = ik\eta\int\int_S[\mathbf{J}_S(\mathbf{r}')G(R_0)+\frac{1}{k^2}(\mathbf{J}_S(\mathbf{r}')\cdot\nabla')\nabla' G(R_0)]dS'. \tag{27}$$

Here

$$\mathbf{J}_S \cdot \nabla' = J_{Sr}\frac{\partial}{\partial r'} + \frac{1}{r'\sin\alpha}J_{S\phi}\frac{\partial}{\partial \phi'},$$

$$G(R_0) = \frac{e^{ikR_0}}{4\pi R_0}$$

and, in terms of the fixed Cartesian unit vectors,

$$\nabla' G(R_0) = \frac{1}{R_0}\frac{d}{dR_0}\left(\frac{e^{ikR_0}}{4\pi R_0}\right) \cdot [r'\sin\theta'(\hat{\mathbf{x}}\cos\phi' + \hat{\mathbf{y}}\sin\phi') + (r'\cos\theta' - r)\hat{\mathbf{z}}].$$

Thus, after noting that

$$\mathbf{J}_S(\mathbf{r}') = J_{Sr}[(\hat{\mathbf{x}}\cos\phi' + \hat{\mathbf{y}}\sin\phi')\sin\alpha + \hat{\mathbf{z}}\cos\alpha] + J_{S\phi}[(-\hat{\mathbf{x}}\sin\phi' + \hat{\mathbf{y}}\cos\phi'],$$

$$\frac{1}{k^2R_0}\frac{d}{dR_0}\left(\frac{e^{ikR_0}}{R_0}\right) = \frac{e^{ikR_0}}{R_0}\left(\frac{i}{kR_0} - \frac{1}{k^2R_0^2}\right),$$

$$(r - r'\cos\alpha)\frac{\partial}{\partial r'}\left[\frac{1}{k^2R_0}\frac{d}{dR_0}\left(\frac{e^{ikR_0}}{R_0}\right)\right] = \left(\cos\alpha - \frac{rr'}{R_0^2}\sin^2\alpha\right)\frac{e^{ikR_0}}{R_0}\left(1 + \frac{3i}{kR_0} - \frac{3}{k^2R_0^2}\right),$$

it follows by substitution of these identities and (13) into (26) and (27) that

$$\mathbf{H}^s(r,0) = -\frac{2iE^{0i}}{\pi\eta}\hat{\mathbf{y}}\int_a^b [kr\sin\alpha\, j_{r1}(r') - k(r - r'\cos\alpha)j_{\phi 1}(r')] \cdot \left(\frac{i}{kR_0} - \frac{1}{k^2R_0^2}\right)\frac{e^{ikR_0}}{R_0}kr'\sin\alpha\, dr', \tag{28}$$

$$\mathbf{E}^s(r,0) = \frac{2}{\pi}E^{0i}\int_a^b \left\{\left(1 + \frac{3i}{kR_0} - \frac{3}{k^2R_0^2}\right) \cdot \left[i\hat{\mathbf{z}}\frac{rr'\sin^2\alpha}{R_0^2}j_{r0}(r') + \hat{\mathbf{x}}\frac{(r - r'\cos\alpha)}{R_0^2}r\sin\alpha\, j_{r1}(r') - \hat{\mathbf{x}}j_{\phi 1}(r')\right] - [i\hat{\mathbf{z}}\cos\alpha\, j_{r0}(r') + \hat{\mathbf{x}}\sin\alpha\, j_{r1}(r') - \hat{\mathbf{x}}j_{\phi 1}(r')] \cdot 2\left(\frac{i}{kR_0} - \frac{1}{k^2R_0^2}\right)\right\}\frac{e^{ikR_0}}{R_0}kr'\sin\alpha\, dr'. \tag{29}$$

Evidently, the axisymmetric component of the radially directed surface current generates an axial electric field while the first Fourier components of both surface currents generate electric and magnetic fields normal to the axis, in accordance with the prescribed polarization.

## IV. Results and Physical Interpretation

In addition to the rigorous mathematical limit $\sin\alpha \to 0$, $a\sin\alpha \to A$, and $b - a \to 2L$, the numerical implementation of this frustum analysis is tested with the limiting case $kb = 520$, $ka = 500$ and $\alpha = 0.002$(rad). This extremely acute and distended frustum is a reasonably close approximation to the circular tube with $kL = 10$ and $A/L = 0.1$ that the authors studied previously [1]. Numerical agreement exists between both the surface currents and the on-axis radial electric field ($E_r = E_z$ when $\theta = 0$) of the independent tube and frustum computations.

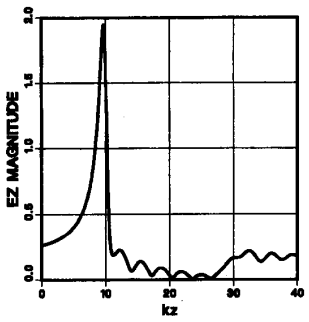


Fig. 2. Magnitude of on-axis $E_z$ for $\beta = 10°, \alpha = 4°$, $kb = 30$, $b/a = 3$.

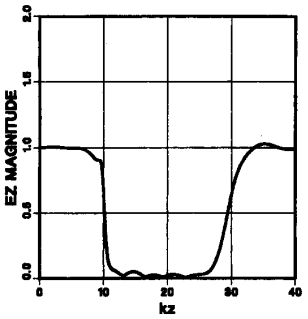


Fig. 3. Magnitude of on-axis $E_z$ for $\beta = 90°$, $\alpha = 4°$, $kb = 30$, $b/a = 3$.

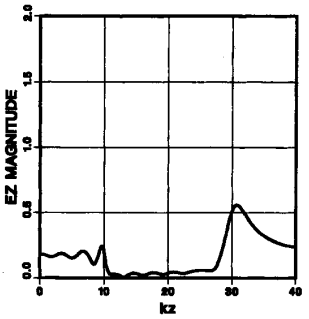


Fig. 4. Magnitude of on-axis $E_z$ for $\beta = 170°$, $\alpha = 4°$, $kb = 30$, $b/a = 3$.

Graphical results for the total axial electric field $|E_z(0,0,z)|$ are presented below for two frusta with identical radial dimensions, $kb = 30$ and $ka = 10$, but cut from cones having different half angles $\alpha = 4°$ and $30°$. The polar angle of incidence $\beta$ of the plane wave is varied through $10°, 90°$, and $170°$ for the narrow frustum ($\alpha = 4°$) in Figs. 2–4. The interval $10 < kz < 30$ is roughly interior to the open scatterer. Electric field intensity is measured relative to the incident wave amplitude $E^{0i}$ of (3). In Figs. 5 and 6, the variation of

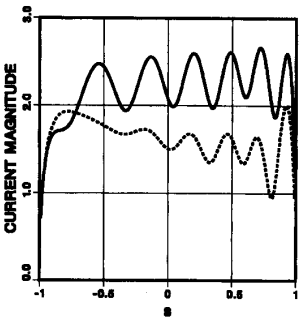


Fig. 5. Magnitude of $J_{Sr}$ for $\beta = 170°$, $\alpha = 4°$, $kb = 30$, $b/a = 3$; $\phi = 0$: solid, $\phi = \pi$: dashed.

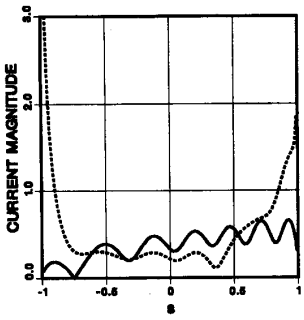


Fig. 6. Current magnitude for $\beta = 170°$, $\alpha = 4°$, $kb = 30$, $b/a = 3$, $\phi = \pi/2$; $J_{Sr}$: solid, $J_{S\phi}$: dashed.

the induced electric current density on the conducting surface is graphically displayed for three azimuthal angles when the exciting plane wave is incident from the direction that subtends an angle 10° with the axis directed out of the narrow end of the frustum, i.e., $\beta = 170°$. Since (3) implies that the excitation is incident in the $\phi = 0$ half-plane, the radial current $J_{Sr}$ of Fig. 5 for $\phi = 0$ (solid curve) is along the directly illuminated line in the plane of incidence. When $\phi = \pi$ (dashed curve), the radial current is along the diametrically opposite or shadowed side of the frustum. Both $J_{Sr}$ (solid curve) and $J_{S\phi}$ (dashed curve) are present in the intermediate ($\phi = \pi/2$) plane depicted in Fig. 6. Surface current density is normalized by the incident magnetic field intensity $E^{0i}/\eta$.

The electrical radius $kA$ of the conical surface, measured transverse to $z$, varies linearly from a minimum value of 0.7 at the narrow end ($r = a$) to a maximum value of 2.1 at the wide end ($r = b$). The most striking difference between the results for this relatively narrow frustum (total radial extent $kb - ka = 20$) and the circular tube of [1] (total longitudinal extent $2kL = 20$ and electrical radius $kA = 1$) is the substantial penetration of the field into the whole interior of the frustum. In the case of the uniform circular tube [1], the on-axis field decays exponentially into the deep interior whenever the cross section is small enough to exclude any propagating (cut-on) waveguide modes. The eigenfunctions/modes of a uniform transmission line, such as the circular tube, have sharp cut-off frequencies below which the field is evanescent and above which unattenuated propagation occurs. For example, the lowest order axisymmetric mode ($TM_{01}$) of the circular waveguide is cut off for $kA < 2.405$. In contrast, the modes of a nonuniform transmission line, such as the conical waveguide [6] of Fig. 1 experience a gradual transition from propagation to evanescence, as a function of electrical distance $kr$. For simplicity, attention is centered presently on the axial ($\theta = 0$) component $E_r$, which exists only for the axisymmetric (azimuthal index $n = 0$) TM to $r$ modes [6]:

$$E_r(r,\theta) \propto \frac{\nu(\nu+1)}{r^2}\hat{H}_\nu^{(1,2)}(kr)P_\nu(\cos\theta)$$

where the index $\nu$ is determined by the boundary condition $P_\nu(\cos\alpha) = 0$. At large $kr \gg \nu$, these waves freely propagate in the $\pm\hat{\mathbf{r}}$ direction, while they are mostly evanescent for small $kr \ll \nu$. Therefore, real nonzero time-average power flow does occur in a conical waveguide that is smaller in cross section than any cut-on circular waveguide at the same frequency of operation. This observation can also be qualitatively explained by considering the oppositely directed evanescent waves that are excited at the cascaded junctions of successively larger but still indivdually cut off circular waveguides that form a stepped approximation to the cone. Effectively, then, the conical scatterer tends to focus a portion of the energy of the incident radio wave, at least in comparison to the uniform tubular scatterer.

In Fig. 2 ($\beta = 10°$), note the high value $E_z/E^{0i} \simeq 2$ near $kz = 10$ due to close proximity to the knife edge at $r = a$. Two other effects contribute to this high field intensity: the narrowing of the cone and hence a focusing at this end, and the larger surface current maxima at the exit end in all cases, including the uniform tube [1]. Between $kz = 10$ and $kz = 30$, the axial field is clearly a damped standing wave whose envelope decays as $r^{-2}$. In the backscattered exterior region ($kz > 30$), the sum of the uniform incident field and the oppositely directed scattered field produces a standing wave pattern consisting of damped oscillations about the value $E_z/E^{0i} = \sin\beta$. The total field is strictly propagating away from the smaller end of the frustum in the forward direction ($kz < 10$), so this field decays almost monotonically from its high value near the edge ($kz = 10$) to the incident value $E_z/E^{0i} = \sin\beta$. This exterior behavior of the frustum is qualitatively identical to that of the circular tube [1].

The axial electric field of Fig. 4, generated by excitation from the complementary direction $\beta = 170°$, exhibits the same general characteristics as in Fig. 2. Observe, however, that in Fig. 4 the peak value, near the exit edge at $kz \simeq 30$, is $E_z/E^{0i} \simeq 0.6$, which is less than the axial maximum of 2 in Fig. 2. This is both reasonable and expected since the frustum axis runs closer to the static singularity at the narrow end than at the wide end. Fig. 3 illustrates the variation of the axial electric field for the intermediate angle $\beta = 90°$. The surface currents displayed in Figs. 5 and 6 are slightly distorted versions of the comparable tube currents of [1]. Note that the natural variable $s = \ln(r^2/ab)/\ln(b/a)$, defined by (16), is the abscissa for graphs of frustum current. In Fig. 5, the six identifiable current oscillations about the physical optics value 2 are distributed down the conducting frustum of

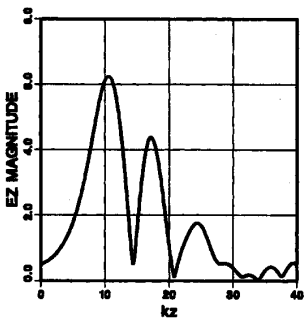


Fig. 7. Magnitude of on-axis $E_z$ for $\beta = 10°, \alpha = 30°, kb = 30, b/a = 3$.

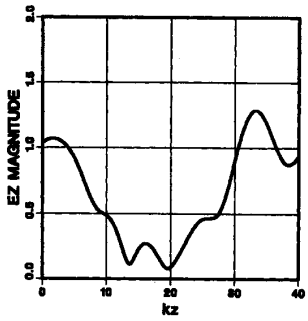


Fig. 8. Magnitude of on-axis $E_z$ for $\beta = 90°, \alpha = 30°, kb = 30, b/a = 3$.

length $b - a \simeq 3\lambda$. The tendency for the oscillations to be higher toward the exit end ($s \rightarrow +1$) of the uniform tube [1] is mostly cancelled by the opposing effect of the increasing surface area over which the current is distributed.

The wider frustum of half-angle $\alpha = 30°$ is subjected to the same onslaught of plane waves from $\beta = 10°$, 90°, and 170°, and the resulting graphs of the axial field are displayed in Figs. 7–9, respectively. The electrical radius $kA$ now varies from 5 to 15, and the greater penetration into this quite open structure is expected. Fig. 7 depicts a resonance condition when $\beta = 10°$, which is evidently not excited when the plane wave is incident from the narrow end as in Fig. 9 for $\beta = 170°$. This is consistent with a geometrical optics view of ray bouncing, whereby the focusing of the field occurs when the plane wave is incident upon a more concave scatterer, i.e., from the wide end. Of course, this moderately large (in terms of wavelength) and more complex frustum geometry also experiences excitable resonances, just like the simpler thin tube of length $\lambda/2$ subjected to broadside TM polarization [1]. The surface currents displayed in Figs. 10 and 11 are qualitatively similar to those of Figs. 5 and 6 for the narrow frustum. One noticeable difference occurs between Figs. 11 and 6, where the azimuthal surface current $|J_{S\phi}|$ is much larger on the wide frustum which can better support such currents. Away from the narrow end, $|J_{S\phi}|$ of Fig. 11 (dashed curve) oscillates about the value $2\sin\alpha = 1$, as expected according to the physical optics approximation.

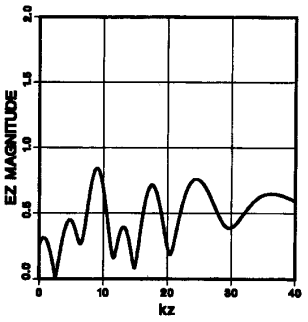


Fig. 9. Magnitude of on-axis $E_z$ for $\beta = 170°$, $\alpha = 30°$, $kb = 30$, $b/a = 3$.

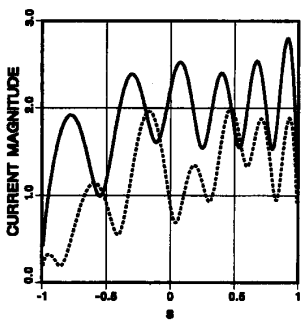


Fig. 10. Magnitude of $J_{Sr}$ for $\beta = 170°$, $\alpha = 30°$, $kb = 30$, $b/a = 3$,; $\phi = 0$: solid, $\phi = \pi$: dashed.

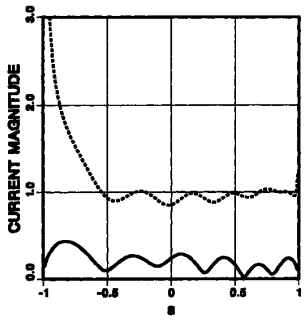


Fig. 11. Current magnitude for $\beta = 170°$, $\alpha = 30°$, $kb = 30$, $b/a = 3$, $\phi = \pi/2$; $J_{Sr}$: solid, $J_{S\phi}$: dashed.

## V. Conclusion

Induced vector currents on the frustum can exhibit extreme variation over the conducting surface, in both the azimuthal and radial directions. In most respects, the scattering by the frustum is a distortion of that by the circular tube. One important difference is the internal focusing effect that is predominantly experienced when the exciting plane wave is incident from the wide end of the frustum. Due to the absence of sharp cut-off frequencies for the nonuniform conical waveguide, the interior of the frustum can support nontrivial field amplitudes, even in regions of relatively small electrical cross section.

## REFERENCES


[1] A. M. J. Davis and R. W. Scharstein, "Electromagnetic plane wave excitation of an open-ended, finite-length conducting cylinder," *J. Electromagn. Waves Appl.*, vol. 7, pp. 301–319, 1993.

[2] H. M. Lee, "Double series expansion of the Green's function for a perfectly conducting tubular cylinder of finite length," *Radio Sci.*, vol. 18, pp. 48–56, 1983.

[3] H. M. Lee, "Electromagnetic scattering of tubular cylindrical structure-double series formulation and some results," *IEEE Trans. Antennas Propagat.*, vol. 35, pp. 384–390, 1987.

[4] K. D. Trott, P. H. Pathak, and F. A. Molinet, "A UTD type analysis of the plane wave scattering by a fully illuminated perfectly conducting cone," *IEEE Trans. Antennas Propagat.*, vol. 38, pp. 1150–1160, 1990.

[5] M. S. Narasimhanand and K. S. Balasubramanya, "Transmission characteristics of spherical TE and TM modes in conical waveguides," *IEEE Trans. Microwave Theory Tech.*, vol. MTT-22, pp. 965–970, 1974.

[6] R. F. Harrington, *Time-Harmonic Electromagnetic Fields*. New York: McGraw-Hill, 1961, p. 280.

[7] A. Ishimaru, *Electromagnetic Wave Propagation, Radiation, and Scattering*. Englewood Cliffs, NJ: Prentice, 1991, p. 355.

[8] P. M. Morse and H. Feshbach, *Methods of Theoretical Physics II*. New York: McGraw-Hill, pp. 1330 (corrected), 1953.

[9] M. Abramowitz and I. Stegun, *Handbook of Mathematical Functions*. Washington, DC: Nat. Bureau. Stand. Appl. Math. Series. 55, 1964, p. 559.


**Anthony M. J. Davis** was born in 1939 in London, UK. He received the B.A. degree in 1960, and the Ph.D. degree in 1964, both from Cambridge University, Cambridge, UK.

He was a Lecturer and later Reader in Mathematics at University College, London, from 1965 to 1984, and in 1977 was awarded the D.Sc. degree by London University for his work on surface waves. He has been Professor of Mathematics at the University of Alabama, Tuscaloosa, since 1985.

Dr. Davis' more recent papers discuss slow viscous flows and electromagnetic wave scattering..

**Robert W. Scharstein** (S'79–M'81–S'86–M'86–SM'94) was born in Covington, KY, in 1955. He received the B.S. degree from the State University of New York, Buffalo, in 1978, and the M.S. degree in 1981 and the Ph.D. degree in 1986 from Syracuse University, Syracuse, NY.

He has been an Engineer with the General Electric Company, an Assistant Professor with Clemson University, and a Senior Engineer with the Sensis Corporation. Since 1989 he has been with the University of Alabama, Tuscaloosa, where he is now Associate Professor of Electrical Engineering, with research interest in electromagnetic and acoustic scattering.